2024 IEEE International Conference on Robotics and Automation (ICRA)
May 13-17, 2024. Yokohama, Japan

2024 IEEE International Conference on Robotics and Automation (ICRA) | 979-8-3503-8457-4/24/$31.00 ©2024 IEEE | DOI: 10.1109/ICRA57147.2024.10610191

An adaptable ankle trajectory generation method for lower-limb exoskeletons by means of safety constraints computation and minimum jerk planning

Raffaele Giannattasio[1], Stefano Maludrottu[2], Gaia Zinni[2], Elena De Momi[3], Matteo Laffranchi[2], Lorenzo De Michieli[2]

***Abstract*— This paper presents a method to compute smooth ankle trajectories for lower limb exoskeletons with powered ankle joints. The proposed approach defines ankle trajectories using four polynomial functions, each representing one of the four primary phases of gait. These polynomials are computed according to different safety constraints. During the single support phase, ground contact constraints are enforced. In the swing phase, an optimization problem is solved to achieve minimum jerk planning while respecting a set of equality and inequality constraints designed to minimize the risk of stumbling. The used approach focuses on making the ankle joint able to smoothly adapt in real-time to different walking styles defined by user-selected gait parameters such as step length and clearance. The primary aim is to improve the user experience by producing a secure and comfortable walking pattern. To validate the effectiveness of the proposed method, the new ankle trajectories were tested on a group of healthy volunteers using the TWIN lower limb exoskeleton.**

I. INTRODUCTION

Spinal cord injury (SCI) [1] and stroke [2] are the two leading causes of acquired disability in adults that often cause the loss, partial or complete, of the ability to move the limbs. An impairment of the mobility of the lower limbs leads in turn to several clinical complications such as muscle atrophy and osteoporosis [1]. In this scenario, repetitive and task-oriented movements of the impaired limbs can improve muscular activity and provide positive effects on cognitive and gait functions, especially in stroke patients [3]. The need to have more effective rehabilitation methods has led researchers to develop over the years a wide range of robotic solutions [4]. Among these, lower-limb exoskeletons are valuable tools in rehabilitation, providing multiple benefits such as muscle strengthening, improved walking speed and efficiency, and addressing secondary medical conditions like spasticity and changes in the cardiovascular system [5]. Most exoskeletons like Hal [6], Ekso [7] and Indego [8] have two active joints for each leg, generally actuated by electrical motors, to perform hip and knee flexion-extension and use passive elements, sometimes in combination with flexible soles [9] for the ankle-foot complex. The gait trajectories implemented in many of these exoskeletons often confine patients to follow rigid and predetermined paths, whose characteristics have several dissimilarities compared with the human walk [10]. For this reason, one of the primary challenges in the field of robotic exoskeletons is to create gait trajectories that accurately replicate human gait behavior, prioritize user comfort, and have the flexibility to adapt to various walking styles, enabling a wide range of movements [11]. In recent years, certain trajectory planning methods have tackled this challenge by defining gait trajectories using a set of *via points*, scaled by user-defined variables called *style parameters*, thereby enabling the generation of a wide set of trajectories. In this context, Mendoza-Crespo et al. [12] define the gait pattern as the spline function passing through seven via points defined as *key events*. Then analyze data from healthy subjects, that have been gathered through a series of multiple tests involving varying step lengths, to derive a linear regression model used to scale the via points. Zuccati et al. in [13] describe the gait pattern using four Bézier curves defined by a set of *control points* properly tuned to achieve smooth and comfortable motion. The desired step length and clearance are used to properly scale the *control point* and reshape the gait pattern. These methods are effective in emulating different walking patterns. However, they do not consider the motion of the ankle joint, posing a safety concern for patients in terms of stumbling risk. Recently in the field of robotics rehabilitation, there has been a notable shift towards the utilization of exoskeletons equipped with active ankle joints. Among the proposed solutions: BioMot [14], H2 [15], and Mina [16] are the most known. Nonetheless, there is a noticeable gap in the literature regarding the implementation of a trajectory planning method that can effectively combine the advantages of using scalable walking patterns and the utilization of an active ankle to achieve safe and more comfortable walks. For instance, in [17], the authors utilize the active ankle to implement powered toe-off motion during the final part of the single support phase. However, there is a notable absence of discussion regarding how the trajectory of the ankle ensures safety and prevents stumbling. To fill this gap, in this article, we introduce an adaptable ankle trajectory generation method, that, by means of safety constraint computation and minimum jerk planning, creates ankle trajectories that are compatible with multiple walking styles. This not only minimizes the risk of stumbling but also results in a smooth motion of the ankle during the walking process. Lastly, we conducted tests using the TWIN lower limb exoskeleton to evaluate the effectiveness of the proposed method. These

[1]Raffaele Giannattasio is with Italian Institute of Technology and Politecnico di Milano raffaele.giannattasio@iit.it
[2]Authors are with Italian Institute of Technology
[3]Author is with Politecnico di Milano

tests involved three healthy subjects under different walking patterns. This paper is structured in the following way: Section II describes the TWIN exoskeleton together with the kinematic model used to represent it. Section III shows the method used to generate scalable gait trajectories used in the TWIN exoskeleton. Section IV provides a comprehensive explanation of the proposed ankle trajectory generation method, along with its real-time implementation on the machine. Finally, in Section V and VI the experimental data are shown and the conclusions are discussed.

II. TWIN EXOSKELETON

TWIN [18]-[19], is a lower-limb exoskeleton developed by the Rehab Technologies Lab at the Italian Institute of Technology (IIT). It has a modular structure and consists of six actuated joints at the hips, knees, and ankles. The actuation units of the hip and knee joints are powered by the BMS-1712-A frameless motors coupled with 80:1 and 50:1 gearboxes respectively. The active ankle joints are powered by the ILM50x14 frameless motors with an overall gear ratio of 140:1 and a total efficiency of less than 50% making the mechanism non-backdrivable. The TWIN exoskeleton is operable via a mobile app that allows the operator to set the desired walking style. The app communicates through Wi-Fi with a central control unit (CCU) located in the device's backpack. This CCU is tasked with generating joint targets, which are subsequently transmitted to the motors via the CAN bus at a frequency of 500 Hz. The motors are then locally controlled in position using a proportional-integral controller.

A. TWIN kinematics

The TWIN kinematic model is a floating-based model [20] composed of two identical 3-DOF open loop chains independent from each other. In Fig.1 q_H, q_K, and q_A represent the joint angles of hip, knee, and ankle, while L_T, L_S and L_F, represent the lengths of thigh, shank, and foot. For the hip and knee joints, the rotation axis is oriented such that the angle is considered negative when the leg is moving backward. For the ankle joint, the rotation axis is oriented such that the angle is considered zero when the foot is perpendicular to the shank, positive when the foot approaches the shank (*dorsiflexion*), and negative when the foot moves away from the shank (*plantarflexion*). The end effector is positioned on the foot tip described by (x_A, z_A), which from direct kinematics is computed by Eq. (1), where (x_M, z_M) are the coordinates of the malleolus.

$$\begin{pmatrix} x_A \\ z_A \end{pmatrix} = \begin{pmatrix} x_M \\ z_M \end{pmatrix} + L_F \begin{pmatrix} \cos(q_H + q_K + q_A) \\ \sin(q_H + q_K + q_A) \end{pmatrix} \quad (1)$$

The reference gait trajectory is planned for (x_M, z_M) using the method described in Section III, and the joint trajectories for q_H and q_K are computed using Eq.(2) and Eq. (3) respectively.

$$q_K = \cos^{-1}\left(\frac{x_M^2 + z_M^2 - L_S^2 - L_T^2}{2L_T L_S}\right) \quad (2)$$

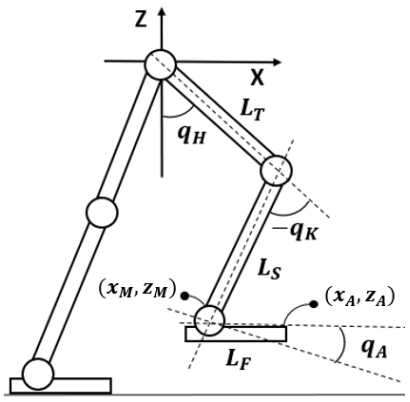

Fig. 1. Floating base kinematic model of TWIN.

$$q_H = \tan^{-1}\left(\frac{z_M}{x_M}\right) - \tan^{-1}\left(\frac{L_S \sin(q_K)}{L_T + L_S \cos(q_K)}\right) \quad (3)$$

These equations are obtained by solving the inverse 2-DOF kinematic problem for the reduced kinematic chain that has (x_M, z_M) as the end-effector by using the cosine rule. The reference trajectory of joint q_A is then planned directly in the joint space using the method described in Section IV.

III. TWIN GAIT TRAJECTORIES

The TWIN gait trajectory describes the cartesian position of the malleolus during the gait [13]. It is divided into four consecutive phases following the human gait cycle. Moreover, it is modeled according to a combination of two style parameters: the step length (SL) which is defined as the distance covered in one step, and the clearance (CL) which is defined as the maximum distance between the malleolus of the swing foot and the ground.

A. The human gait

The human gait cycle (also defined as *stride*) [21]-[22], as shown in Fig. 2, is a periodic sequence of two steps. It is composed of four consecutive phases, called initial double support (ids), single support (ss), final double support (fds), and swing (sw). The single support and swing phases each comprise approximately 40% of the gait cycle, during which one leg maintains ground contact (ss) while the other is in mid-air (sw). The initial and final double support phases, accounting for roughly 10% of the cycle, involve both legs simultaneously in contact with the ground. These phases commence with one foot making contact with the ground (*Heel strike*) and conclude when the opposite foot lifts off the ground (*Toe off*). The ids denotes the behavior of the leg landing on the ground, while fds describes the behavior of the opposite leg lifting off the ground.

B. TWIN gait trajectories

The gait trajectory of TWIN, inspired by the work of Hyunn et al. [23], is computed taking into account the subdivision of the human gait explained in the previous

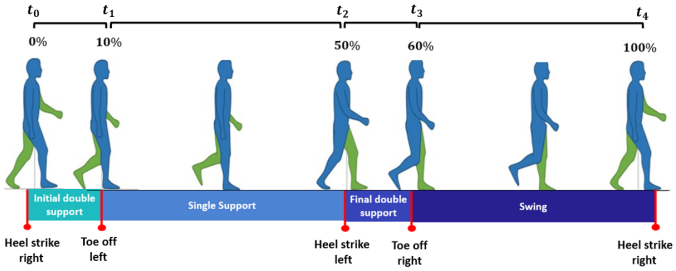

Fig. 2. Human gait cycle for the right leg.

subsection. Each phase of the gait is modeled using a 2-dimensional n-degree Bézier curve of equation:

$$B^n(\tau) = \sum_{i=0}^{n} \frac{n!}{i!(n-1)!}(1-\tau)^{n-i}\tau^i P_i \quad \forall\, \tau \in [0,1] \quad (4)$$

Where τ is a parametric variable obtained by mapping the time interval for each of the four gait phases over the interval $[0,1]$. P_i is a set of cartesian points called *control points* that define the mathematical representation of the curve. To compute the entire gait trajectory the four curves are combined together forming a Piece-wise Bézier function as defined by $S(t)$ in Eq.(5):

$$S(t) = \begin{cases} B^n_{ids}(t) & \forall\, t \in [t_0, t_1[\\ B^n_{ss}(t) & \forall\, t \in [t_1, t_2[\\ B^n_{fds}(t) & \forall\, t \in [t_2, t_3[\\ B^n_{sw}(t) & \forall\, t \in [t_3, t_4] \end{cases} \quad (5)$$

The time intervals in which the four curves are defined are computed according to the temporal relation described in Eq. (6).

$$\begin{cases} t_1 - t_0 = t_3 - t_2 = kT \\ t_2 - t_1 = t_4 - t_3 = (1-k)T \end{cases} \quad (6)$$

Where $k = 0.1$, and T is the time duration of one step. T is also used as time delay to identify the position of the two legs, i.e. if one leg is following a gait trajectory $S(t)$ for symmetry the other leg will follow the gait trajectory $S(t \pm T)$.

As described in [13], a subset of *control points* is chosen to ensure C^3 continuity between the gait phases, while the remaining control points are chosen according to the style parameters SL and CL. This representation gives the possibility to perform a wide range of movements characterized by different step lengths and different clearances by scaling the position of the *control points*. Once computed the gait trajectory, $q_H(t)$ and $q_K(t)$ are derived using inverse kinematics according to Eq. (2) and (3).

IV. Ankle Trajectory Generation Method

The possibility to perform a large set of gait trajectories gives the necessity to design the trajectory of the ankle joint in a manner that ensures the safety of the user across all potential walking patterns. We define the ankle trajectory, $q_A(t)$ using four n-degree polynomials that represent the four main phases of the gait as shown in Eq. (7):

$$q_A(t) = \begin{cases} q^{ids}_A(t) & \forall\, t \in [t_0, t_1] \\ q^{ss}_A(t) & \forall\, t \in [t_1, t_2] \\ q^{fds}_A(t) & \forall\, t \in [t_2, t_3] \\ q^{sw}_A(t) & \forall\, t \in [t_3, t_4] \end{cases} \quad (7)$$

where the generic n-degree polynomial is described as in Eq. (8):

$$q(t) = a_0 + a_1 t + a_2 t^2 + \cdots + a_{n-1} t^{n-1} \quad (8)$$

The hip and knee joint trajectories are leveraged to establish safety constraints that must be applied to the ankle joint throughout the gait cycle. These constraints are subsequently incorporated into an optimization problem aimed at uncovering a secure and comfortable ankle trajectory. We denote with a_{ids},a_{ss}, a_{fds}, and a_{sw} the sets of coefficients that define the four polynomials. In the subsequent subsections, we will provide a detailed explanation of how these coefficients are derived for each phase of the gait.

A. Single support polynomial

During the single support phase, the foot maintains full contact with the ground, thus imposing a kinematic constraint on the ankle. Referring to Fig. 1, imposing a constraint of full contact with the ground implies ensuring that the position of the malleolus and the foot tip are aligned along the z-axis, as shown in Eq. (9).

$$z_A(t) = z_M(t) \quad (9)$$

Substituting Eq. (1) into Eq. (9) and solving for $q_A(t)$, the relation Eq. (10) is obtained.

$$q_A(t) = -(q_H(t) + q_K(t)) \quad (10)$$

Where $q_H(t)$ and $q_K(t)$ are computed from $(x_M(t), z_M(t))$ by inverse kinematics using the Eq. (2) and Eq. (3). Finally, substituting Eq. (8) into Eq. (10) we obtain the following constraint function:

$$a_0 + a_1 t + a_2 t^2 + \cdots + a_{n-1} t^{n-1} = -(q_H(t) + q_K(t)) \quad (11)$$

Since the trajectory must respect this constraint for the entire duration of the single support phase, Eq. (11) is evaluated for m different values of $t \in [t_1, t_2]$ deriving a set of constraints equation that in matrix form can be written as follows:

$$V \cdot a = c \quad (12)$$

where a and c are respectively $\mathbb{R}^{n\times 1}$ and $\mathbb{R}^{m\times 1}$ column vectors:

$$a = \begin{bmatrix} a_0 \\ \vdots \\ a_n \end{bmatrix} \quad c = \begin{bmatrix} -(q_H(t_1) + q_K(t_1)) \\ \vdots \\ -(q_H(t_2) + q_K(t_2)) \end{bmatrix} \quad (13)$$

and V is a $\mathbb{R}^{m\times n}$ Vandermonde matrix:

$$V = \begin{bmatrix} 1 & t_1 & \cdots & t_1^{n-1} \\ \vdots & \vdots & \ddots & \vdots \\ 1 & t_2 & \cdots & t_2^{n-1} \end{bmatrix} \tag{14}$$

To compute q_A^{ss} we employ an 8^{th} degree polynomial and a value of $m = 50$, that has been empirically determined to closely represent the variability of the Eq. (10) over the single support time duration. Since $n = 8$ and $m >> n$, the system is indeterminate. The problem is therefore solved as a least squares problem, finding the vector of coefficients a_{ss} as in Eq. (15):

$$a_{ss} = \min_a |c - V * a|^2 \tag{15}$$

that have the following solution:

$$a_{ss} = V^{*-1}c = (V^T V)^{-1} V^T c \tag{16}$$

To solve Eq. (16) we factorize V as a product of an orthogonal matrix Q and an upper triangular matrix R using QR factorization [24]. With this factorization, the calculation of the pseudo-inverse of V is simplified, and the solution becomes easy to compute in real time. Using an 8^{th} degree polynomial gives us the maximum error between q_A^{ss} and the interpolated data of $e = 1.5 \times 10^{-4} rad$.

B. Swing polynomial

The swing polynomial is computed via minimum jerk trajectory planning [25]. Jerk is the time derivative of acceleration and it is related to the smoothness of the motion [26]. Minimum jerk trajectories are widely used in robotics, including rehabilitation scenarios, to generate comfortable and smooth motions [27]-[28]. The following section explains how the optimization problem is posed and implemented into the TWIN exoskeleton.

1) Optimization problem: To compute $q_A^{sw}(t)$ we use a 7^{th} degree polynomial whose coefficients a_{sw} are computed by solving an optimization problem, as shown in Eq. (17).

$$a_{sw} = \min_a \int_{t_3}^{t_4} |\ddot{q}_A(a,t)|^2 \tag{17}$$

Subject to the following set of equality and inequality conditions:

$$\begin{cases} q_A^{sw}(t_3) = p_i \\ \dot{q}_A^{sw}(t_3) = v_i \\ \ddot{q}_A^{sw}(t_3) = a_i \\ q_A^{sw}(t_4) = p_f \\ \dot{q}_A^{sw}(t_4) = v_f \\ \ddot{q}_A^{sw}(t_4) = a_f \end{cases} \quad \begin{cases} q_A^{sw}(t) > c_1(t) \\ q_A^{sw}(t) > c_2(t) \\ q_A^{sw}(t) < c_3 \end{cases} \tag{18}$$

Where (p_i, v_i, a_i) and (p_f, v_f, a_f) are respectively the position, velocity, and acceleration imposed at the start and the end of the swing. While $(c_1(t), c_2(t), c_3)$ are the inequality constraints imposed to ensure safety. Both the equality and inequality constraints are explained in detail in the following subsections.

Fig. 3 shows the optimal trajectory computed for a specific set of constraints.

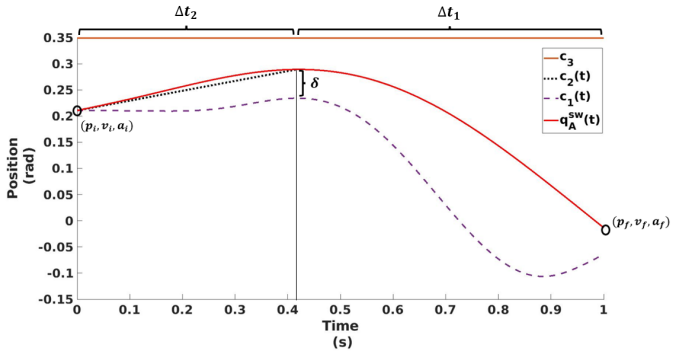

Fig. 3. Optimal swing polynomial trajectory over a normalized swing time, for a specific set of safety constraints computed using $SL = 30cm, CL = 6cm$

2) Inequality constraints computation: The first constraint we introduce, $c_1(t)$, is a safety constraint that defines the minimum ankle angle needed to avoid the ground during the swing phase. During the swing, the ground is defined by the position of the single support foot along the z-axis. To avoid ground contact the end-effector of the swing leg must satisfy the following conditions:

$$z_A(t) > z_M(t - T) \quad \forall t \in [t_3, t_4] \tag{19}$$

Where $z_M(t - T)$ denotes the cartesian position of the malleous during single support. Using Eq. (1) we can rewrite Eq. (19) as follows:

$$z_M(t) + L_F sin(q_H(t) + q_K(t) + q_A(t)) > z_M(t - T) \tag{20}$$

Solving for $q_A(t)$ we derive $c_1(t)$ as follows:

$$c_1(t) = sin^{-1}\left(\frac{z_M(t - T) - z_M(t)}{L_F}\right) - (q_H(t) + q_K(t)) \tag{21}$$

It should be noted, in Fig. 3, that $c_1(t)$ always presents a local maximum. We designate the time at which this maximum occurs as t_c, and we use it to establish a secondary safety constraint, $c_2(t)$, that introduces additional safety distance from the ground during the initial part of the swing where the risk of stumbling is higher. This constraint is defined as the straight line $c_2(t) = mt + q$ that passes through $c_1(t_3)$ and $c_1(t_c) + \delta$, with δ selected to achieve a safety distance of $1.5\ cm$ between the end-effector and the ground at time t_c. Moreover, we divided the swing time into two intervals: $\Delta t_1 = [t_c, t_4]$ and $\Delta t_2 = [t_3, t_c]$, and we impose $q_A^{sw}(t) > c_1(t)\ \forall t \in \Delta t_1$, and $q_A^{sw}(t) > c_2(t)\ \forall t \in \Delta t_2$. Finally, c_3 is set according to the motor operational limit as the maximum angle reachable by the ankle joint, that is $c_3 = 0.35\ rad$. By integrating these three constraints, the ankle trajectory is restricted to a precisely defined angular range during the swing phase. This specified range establishes a safety zone in which the ankle joint begins the swing motion by smoothly augmenting dorsiflexion, ensuring consistent elevation above the ground and adherence to its mechanical thresholds.

3) Equality constraints computation: As defined in Eq. (18), at the beginning and end of the swing phase we impose three constraints on position, velocity, and acceleration. These constraints are designed to ensure smooth transitions between the swing phase and the two double support phases. Since the first point of the swing is the last point for which the foot tip is still in contact with the ground, we impose $p_i = c_1(t_3)$. Furthermore, we set $v_i = \frac{c_1(t_c)-c_1(t_3)}{t_c-t_3}$, that is the minimum velocity compatible with the inequality constraint at t_3. p_f and v_f are chosen empirically to introduce a certain landing angle and velocity of the foot at the beginning of the initial double support phase. Finally, we impose $a_i = a_f = 0$ to mitigate the risk of uncomfortable foot movements during heel strike and toe-off motion.

4) Real time implementation: Constraints $c_1(t)$ and $c_2(t)$ changes for different gait trajectories. As a result, to compute $q_A^{sw}(t)$, a new optimization problem must be solved each time a style parameter changes. This process is computationally demanding and introduces latency whenever a user selects a new combination of parameters. For this reason, we chose to perform an offline computation of the optimization problem. Let's denote with p_m the point obtained evaluating the optimal solution at a certain time $t_m = \frac{t_4-t_3}{2}$. We compute offline the value of p_m for each pair of SL and CL within a predefined subset of style parameters. Moreover, we use the polynomial surface defined in Eq. 22 to describe the relation between the aforementioned p_m and the style parameters.

$$\begin{aligned} p_m(SL, CL) = p_{00} + p_{10}SL + p_{01}CL + p_{20}SL^2 \\ + p_{11}SL \cdot CL + p_{02}CL^2 + p_{30}SL^3 \\ + p_{21}SL^2 \cdot CL + p_{12}SL \cdot CL^2 + p_{03}CL^3 \end{aligned} \tag{22}$$

Where the coefficients are computed minimizing the least square error between all the values of p_m. Given a specific couple of SL and CL, we can use Eq. 22 to derive the value of p_m that, within a margin of approximation, belongs to the optimal solution at time t_m. This point is used to compute in real-time an approximated optimal solution by simply solving the squared system of equation defined adding the constraint equation $q_A^{sw}(t_m) = p_m$ in the equality constraints equations system of Eq. (18). Figure 4(a) shows the spatial representation of the Eq. (22), while figure 4(b) shows the residual errors between the values of p_m computed using Eq. (22) and the values of p_m computed offline over a subset of 2,500 possible combinations of the styles parameter.

From figure 4(b) it is noticeable that the maximum residual error is in the order of $4 \times 10^{-3} rad$. This error produces a low deviation between the optimal and the approximated trajectory, that in terms of maximum jerk deviation, is in the order of $1\ rad/s^3$, which can be considered a negligible perturbation. Moreover, for all the combinations of the style parameters, the inequality constraints are always respected by the approximated solution. It should be further noticed, that using Eq. (22) allows us to save computational resources. Indeed we can represent the optimal solution for an arbitrarily large number of style parameters by using only 10 coefficients.

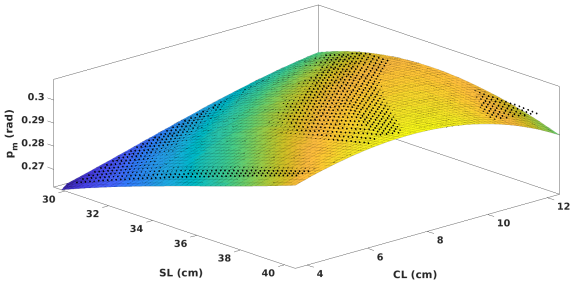

(a)

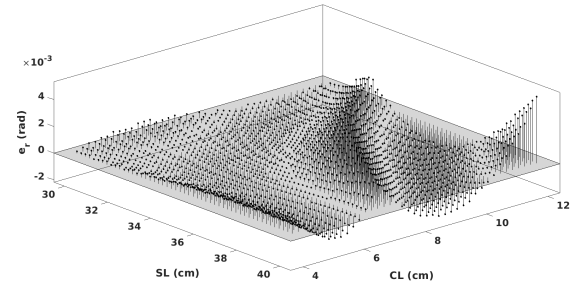

(b)

Fig. 4. (a) Spatial representation of the polynomial surface used to represent the relation between p_m and the style parameters. (b) Residual error between all the value of p_m and their approximation using the polynomial surface.

C. Double support polynomials

To achieve smooth transitions between the four parts of the gait phases, the double support trajectories are computed as the 8^{th} degree polynomials that connect the swing and the single support trajectories ensuring C^4 continuity.

V. Testing and Validation

To evaluate the effectiveness of the proposed ankle trajectory generation method a group of three healthy subjects, who had experience in walking with lower-limb exoskeletons equipped with passive ankle joints, were asked to walk on a level ground performing a variable set of gait trajectories with different CL and gait velocities, where the gait velocity is defined as $v_g = \frac{SL}{T}$ and is measured in m/s.

A. Experimental Setup

The three healthy subjects had an average age of 29 ± 2 years old, an average height of $1.70 \pm 5\,m$, and an average weight of $66 \pm 9\,Kg$. Each subject walks with one combination of parameters (CL and v_g) for a 10-meter Walking Test (10MWT), then the parameters are changed and the subject performs another walk. We choose to perform the experiments at four different walking speeds: low ($0.15\,m/s$), medium ($0.205\,m/s$), high ($0.285\,m/sec$), and the maximum reachable by the exoskeleton ($0.33\,m/s$). According to Louie et al. [29], these speeds are compatible with the mean speed reached with the commercial exoskeletons during rehabilitation for individuals with SCI, which is $0.26\,m/s$. Regarding the clearances, we decided to test $10\,cm$, $8\,cm$,

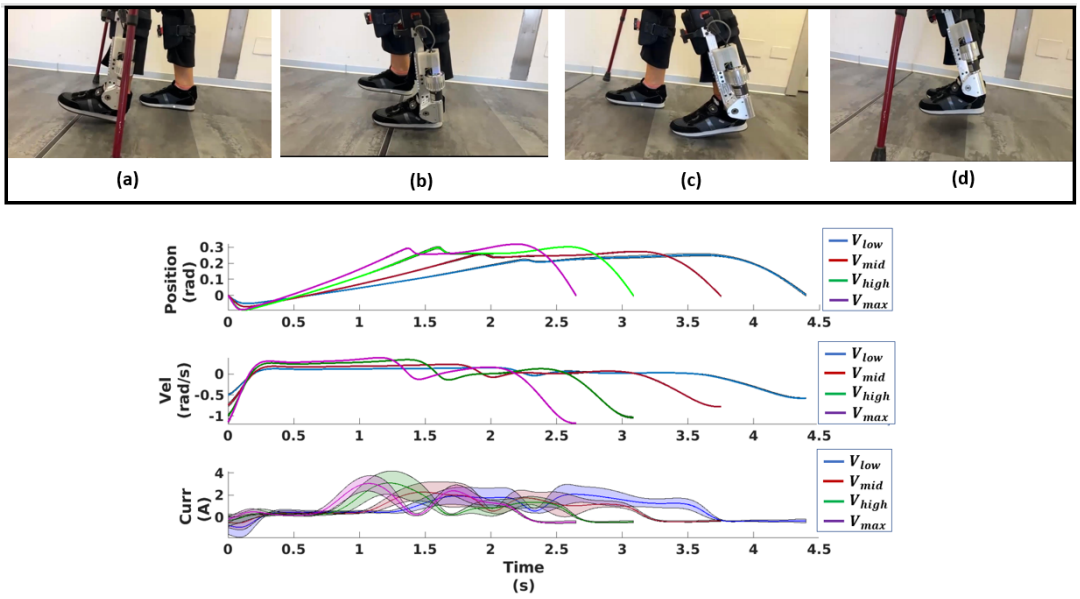

Fig. 5. In the upper part of the figure: Snapshots of the position of the foot tip during experiments performed at low walking speed and $CL = 2$. In particular, the position of the foot tip during the initial double support phase (a), single support phase (b), final double support phase (c), and swing phase (d). In the lower part of the figure: Mean and standard deviation of the experimental data collected for three healthy patients walking at clearance $CL = 2$ for low velocity V_{low}, mid velocity V_{mid}, high velocity V_{high}, and maximum velocity V_{max}.

$6\,cm$, $4\,cm$, and $2\ cm$. All the experiments are performed using the crutches.

B. User Experience and Results

The upper part of Figure 5, shows a sequence of snapshots taken during an experiment. The participants involved in the study appreciated the fluidity of motion during the swing phase and expressed an improved sense of safety when compared to walking with an exoskeleton featuring a passive ankle. In the lower part of Fig. 5, we present the experimental data concerning ankle joint position, velocity, and current collected during the tests with different walking velocities at clearance $CL = 2\ cm$, which is the condition for which the velocity of the ankle joint is the highest. Specifically, we display the average ankle joint position, velocity, and ankle joint currents together with their standard deviation. These averaged values are computed from all the strides observed during the 10MWT performed by all the participants. We observed a position tracking error of $0.04\,rad$, and a maximum joint velocity of $-1.05\,rad/s$, a value consistent with the maximum velocity achieved by the human ankle during slow walking [30]. Furthermore, it becomes apparent that at higher walking speeds, there is a quicker and more pronounced dorsiflexion. This allows users to attain increased ankle engagement simply by increasing the desired walking speed. The variance observed in the averaged current data serves as an indicator of the presence of current spikes, commonly associated with sudden accelerations and discomforting movements [28]. This characteristic makes it a valuable metric for assessing the comfort and fluidity of motion. Notably, in Fig. 5, it is evident that this variance remains consistently low throughout the swing phase across all tested conditions, with a maximum of 0.6A.

VI. Conclusion and Future Works

This paper introduces a method to compute smooth and safe ankle trajectories for lower limb exoskeletons with powered ankle joints. The method proposed, imposes ground contact constraints during the single support phase and computes minimum jerk trajectory that respects safety conditions in real time using low computational resources during the swing. This accomplishment is crucial for minimizing latency during trajectory computation. Such latency could pose challenges for the implementation of future applications in which the gait pattern may need to be adjusted during a walking session based on the user's intended motion. The resulting ankle trajectories were tested on a group of three healthy volunteers under different walking patterns using the TWIN lower limb exoskeleton. Examination of the experimental data indicated a smooth motion of the ankle joint, as evidenced by the notable absence of current spikes. In subsequent research endeavors, our objectives include conducting experiments with a larger and more diverse pool of participants, comprising individuals both with and without gait impairments. Moreover, we endeavor to identify novel metrics for evaluating the efficacy of the proposed method in enhancing gait stability. Additionally, we aim to integrate extra user-defined constraints to regulate the plantarflexion during the final double support phase, offering users enhanced control in shaping their desired ankle motion.

VII. Acknowledgment

This work was supported by the Istituto nazionale per l'assicurazione contro gli infortuni sul lavoro (INAIL) under grant agreement "PR19-RR-P1 - TwinMED" and "PR23-RR-P2 ClinicEXO".

REFERENCES

[1] World Health Organization, International Spinal Cord Society. (2013). International perspectives on spinal cord injury. World Health Organization.

[2] Owolabi, M. O., Thrift, A. G., Martins, S., Johnson, W., Pandian, J., Abd-Allah, F., ... Stroke Experts Collaboration Group. (2021). The state of stroke services across the globe: Report of World Stroke Organization–World Health Organization surveys. International Journal of Stroke, 16(8), 889-901.

[3] Chung, S. H., Kim, J. H., Yong, S. Y., Lee, Y. H., Park, J. M., Kim, S. H., Lee, H. C. (2019). Effect of task-specific lower extremity training on cognitive and gait function in stroke patients: a prospective randomized controlled trial. Annals of Rehabilitation Medicine, 43(1), 1-10.

[4] Díaz, I., Gil, J. J., Sánchez, E. (2011). Lower-limb robotic rehabilitation: literature review and challenges. Journal of Robotics, 2011.

[5] Mekki, M., Delgado, A. D., Fry, A., Putrino, D., Huang, V. (2018). Robotic rehabilitation and spinal cord injury: a narrative review. Neurotherapeutics, 15, 604-617.

[6] Kawamoto, H., Taal, S., Niniss, H., Hayashi, T., Kamibayashi, K., Eguchi, K., Sankai, Y. (2010, August). Voluntary motion support control of Robot Suit HAL triggered by bioelectrical signal for hemiplegia. In 2010 Annual international conference of the IEEE engineering in medicine and biology (pp. 462-466). IEEE.

[7] Kolakowsky-Hayner, S. A., Crew, J., Moran, S., Shah, A. (2013). Safety and feasibility of using the EksoTM bionic exoskeleton to aid ambulation after spinal cord injury. J Spine, 4(003), 1-8.

[8] Farris, R. J., Quintero, H. A., Murray, S. A., Ha, K. H., Hartigan, C., Goldfarb, M. (2013). A preliminary assessment of legged mobility provided by a lower limb exoskeleton for persons with paraplegia. IEEE Transactions on neural systems and rehabilitation engineering, 22(3), 482-490.

[9] Vouga, T., Fasola, J., Baud, R., Manzoori, A. R., Pache, J., Bouri, M. (2022). TWIICE One powered exoskeleton: effect of design improvements on usability in daily life as measured by the performance in the CYBATHLON race. Journal of NeuroEngineering and Rehabilitation, 19(1), 1-10.

[10] Swank, C., Wang-Price, S., Gao, F., Almutairi, S. (2019). Walking with a robotic exoskeleton does not mimic natural gait: A within-subjects study. JMIR rehabilitation and assistive technologies, 6(1), e11023.

[11] Beyaert, C., Vasa, R., Frykberg, G. E. (2015). Gait post-stroke: Pathophysiology and rehabilitation strategies. Neurophysiologie Clinique/Clinical Neurophysiology, 45(4-5), 335-355.

[12] Mendoza-Crespo, R., Torricelli, D., Huegel, J. C., Gordillo, J. L., Pons, J. L., Soto, R. (2019). An adaptable human-like gait pattern generator derived from a lower limb exoskeleton. Frontiers in Robotics and AI, 6, 36.

[13] Zuccatti, M., Zinni, G., Maludrottu, S., Pericu, V., Laffranchi, M., Del Prete, A., De Michieli, L., Vassallo, C. (2023, September). Modeling the human gait phases by using Bèzier curves to generate walking trajectories for lower-limb exoskeletons. In 2023 International Conference on Rehabilitation Robotics (ICORR). IEEE.

[14] Bacek, T., Moltedo, M., Langlois, K., Prieto, G. A., Sanchez-Villamañan, M. C., Gonzalez-Vargas, J., ... Moreno, J. C. (2017, July). BioMot exoskeleton—Towards a smart wearable robot for symbiotic human-robot interaction. In 2017 International Conference on Rehabilitation Robotics (ICORR) (pp. 1666-1671). IEEE.

[15] Bortole, M., Venkatakrishnan, A., Zhu, F., Moreno, J. C., Francisco, G. E., Pons, J. L., Contreras-Vidal, J. L. (2015). The H2 robotic exoskeleton for gait rehabilitation after stroke: early findings from a clinical study. Journal of neuroengineering and rehabilitation, 12, 1-14.

[16] Mummolo, C., Peng, W. Z., Agarwal, S., Griffin, R., Neuhaus, P. D., Kim, J. H. (2018). Stability of mina v2 for robot-assisted balance and locomotion. Frontiers in neurorobotics, 12, 62.

[17] Griffin, R., Cobb, T., Craig, T., Daniel, M., van Dijk, N., Gines, J., ... Neuhaus, P. (2017). Stepping forward with exoskeletons: team IHMC? s design and approach in the 2016 CYBATHLON. IEEE Robotics Automation Magazine, 24(4), 66-74.

[18] Laffranchi, M., D'Angella, S., Vassallo, C., Piezzo, C., Canepa, M., De Giuseppe, S., ... De Michieli, L. (2021). User-Centered design and development of the modular TWIN lower limb exoskeleton. Frontiers in neurorobotics, 129.

[19] Vassallo, C., De Giuseppe, S., Piezzo, C., Maludrottu, S., Cerruti, G., D'Angelo, M. L., ... De Michieli, L. (2020, May). Gait patterns generation based on basis functions interpolation for the TWIN lower-limb exoskeleton. In 2020 IEEE International Conference on Robotics and Automation (ICRA) (pp. 1778-1784). IEEE.

[20] Featherstone, R. (2014). Rigid body dynamics algorithms. Springer.

[21] Kharb, A., Saini, V., Jain, Y. K., Dhiman, S. (2011). A review of gait cycle and its parameters. IJCEM International Journal of Computational Engineering Management, 13, 78-83.

[22] Perry, J., Davids, J. R. (1992). Gait analysis: normal and pathological function. Journal of Pediatric Orthopaedics, 12(6), 81523

[23] Hyun, D. J., Lim, H., Park, S., Yoon, J., Jung, K., Bae, K., Lee, I. (2019). Walking propulsion generation in double stance by powered exoskeleton for paraplegics. Robotics and Autonomous Systems, 116, 24-37.

[24] Anderson, E., Bai, Z., Dongarra, J. (1992). Generalized QR factorization and its applications. Linear Algebra and its Applications, 162, 243-271.

[25] Piazzi, A., Visioli, A. (2000). Global minimum-jerk trajectory planning of robot manipulators. IEEE transactions on industrial electronics, 47(1), 140-149.

[26] Kyriakopoulos, K. J., Saridis, G. N. (1988, April). Minimum jerk path generation. In Proceedings. 1988 IEEE international conference on robotics and automation (pp. 364-369). IEEE.

[27] Amirabdollahian, F., Loureiro, R., Harwin, W. (2002, May). Minimum jerk trajectory control for rehabilitation and haptic applications. In Proceedings 2002 IEEE international conference on robotics and automation (Cat. No. 02CH37292) (Vol. 4, pp. 3380-3385). IEEE.

[28] Mohamad, H., Ozgoli, S., Motawej, F. (2023). Minimum-Time and Minimum-Jerk Gait Planning in Joint Space for Assistive Lower Limb Exoskeleton. Journal of Bionic Engineering, 1-15.

[29] Louie, D. R., Eng, J. J., Lam, T. (2015). Gait speed using powered robotic exoskeletons after spinal cord injury: a systematic review and correlational study. Journal of neuroengineering and rehabilitation, 12(1), 1-10.

[30] Grimmer, M., Seyfarth, A. (2014). Mimicking human-like leg function in prosthetic limbs. Neuro-robotics: from brain machine interfaces to rehabilitation robotics, 105-155.